Inelastic analysis and life assessment of intermediate heat exchanger for fast breeder reactor

Y.Sohman & H.Wada
Mitsubishi Heavy Industries Ltd, Kobe, Japan
T.Igari
Mitsubishi Heavy Industries Ltd, Nagasaki, Japan

1 INTRODUCTION

Intermediate heat exchanger is well known as one of the critical components in fast breeder reactor. Since the tubesheet shows a quick response to the thermal transient of the sodium flowing in the holes of the tubesheet, a high thermal stress occurs at a boundary between rim and tubesheet. Life assessment based on inelastic analysis is often required for the intermediate heat exchanger since an integrity of the structure can not be confirmed by the design method based on elastic analysis. So far, several analytical researches on the integrity of the intermediate heat exchanger have been reported (Van de Graaf et al. 1985). These analysis have been made usually by use of a combination of the ORNL'S constitutive mode (Corum 1974) and life assessment method shown in ASME B & PV Code Case N-47. However, an improvement of this procedure considering the realistic inelastic behavior and failure mechanism of the structural materials has been required to be established. And a reasonable estimation method of macroscopic inelastic behavior of the perforated plates, which is essential to the analysis of tubesheet, is also required.

This paper presents results of inelastic analysis and life assessment of the intermediate heat exchanger subjected to cyclic thermal transient of sodium. A set of improved constitutive model and life assessment method shown in the related papers (Igari et al. 1987 & Sakon et al. 1987) is adopted.

2 DESCRIPTION OF THE PROBLEM

Schematic view of the intermediate heat exchanger of loop-type fast breeder reactor made of type 304 stainless steel is shown in Fig.1. The primary sodium flows downward among the straight tubes, on the other hand, the secondary sodium flows upward in the tubes. There are two tubesheets at both ends of the tubes, and the upper one which is enlarged in the figure is the high-temperature tubesheet to be analysed. The tubesheet has a uniformly distributed triangular penetration pattern of circular holes, with ligament efficiency η of 0.35.

Operation curve adopted here is shown in Fig.2. After the normal start up with heating rate of 25°C/h and subsequent steady operation for 2177 h with the constant sodium temperatures of 510°C (primary) and 475°C (secondary), the manual trip following hot shock and

subsequent down shock with cooling rate of 1°C/S is considered.

3 ANALYSIS METHOD

3.1 FEM modelling of the tubesheet structure

The high-temperature tubesheet shown in Fig.1 was modelled to an axisymmetric body with the equivalent solid plate. Mesh division of the model is shown in Fig.3. Elements adopted are 8-nodes isoparametric ones of general purpose code MARC. Heat transfer by primary and secondary sodiums is considered in the heat conduction analysis. Dead weight and fluid-pressure difference between primary and secondary sodiums ($4Kg/cm^2$) as well as thermal load by the temperature distribution are taken into account in the stress analysis.

3.2 Constitutive equation

The constitutive equation is a classical one which distinguishes between plastic and creep strains, and has a feature to use the simplified nonlinear plasticity model including the continuous cyclic hardening (Igari & Koto et al. 1987), instead of the ORNL'S tenth-cycle hardening model with bilinear stress-strain representation. The plasticity- creep interaction is partially considered in plasticity, and so-called β-option (Corum 1974) is adopted in creep.

3.3 Analysis method of perforated plate

Temperature distribution of perforated plate is assumed to be determined by the heat conduction analysis of unit cell model containing one hole. Consequently, temperature distribution in a plane with the same z-coordinate is uniform. This assumption predicts large temperature distribution at rim-ligament boundary and leads to a conservative strength evaluation of this part.

As for the derivation of the equivalent solid plate properties in the inelastic analysis, the concept of the effective stress is adopted. By carrying out the experimental study on macroscopic creep behavior of perforated plates, one of the authors clarified the fact that the macroscopic minimum creep rate of perforated plates is predictable by effective stress σ_{nom} (Igari et al. 1987). This effective stress is simply estimated for usual structural material by the following equation,

(1) $\quad \sigma_{nom}=E/E^*\sigma^*$

In this paper, an extension of this fact to the case of plasticity as well as the case of creep involving primary and secondary creep is made. Assuming that the creep property of base material exhibiting both primary and secondary creep is expressed by the next equation,

(2) $\quad \varepsilon_c=F(\sigma, T, t)$

the creep property of the equivalent solid plate is assumed to be expressed as follows,

(3) $\quad \varepsilon_c^*=F(\sigma_{nom}, T, t)$

As for plasticity, the same procedure is adopted for the nonlinear property of base material expressed as,

(4) $\varepsilon p = G(\sigma, T, \kappa)$, (κ:Hardening parameter)

assuming that the equivalent solid plate property is shown as follows,

(5) $\varepsilon p^* = G(\sigma_{nom}, T, \kappa)$.

3.4 Life estimation method

Estimation of creep-fatigue damage is basically based on the linear damage rule shown in ASME Boiler and Pressure Vessel Code Case N-47, but the equivalent stress proposed by Huddleston (Huddleston 1985) instead of the equivalent stress by von Mises is adopted in the creep damage calculation in order to estimate the multiaxial creep damage rationally. A trial use of the Strainrange Partitioning method (Manson 1973) is also made here, in order to study the creep-fatigue damage from the view point of strain-based estimation method. The assumption of uniaxialization of FEM results (Sakon et al. 1987) was adopted in both fatigue damage calculation in the linear damage rule and application of SRP method. Accumulated inelastic strain is checked from a view point of consumption of creep ductility (Sakon et al. 1987).

4 RESULTS OF ANALYSIS

Time history of temperature at representative portions of the structure at the hot shock and down shock is shown in Fig.4. Since the perforated plate shows a quick response to the temperature of sodium, there is a large temperature difference between rim and perforated plate. Trajectories of stress at representative two portions of the structure are shown in Fig.5 for both elastic and inelastic cases. The marks in the figure designate the points shown in the operation curve. Stress range for part (I) is prescribed by the pair of stresses at hot shock and down shock, on the other hand, that for part (II) is prescribed by those at normal start up and shut down. These two portions are representative of highly stressed portions where plastic and creep deformation occur. It is found from the figure that a slight non-proportional loading occurs for these portions. At the rim-tubesheet boundaries which are represented by the portion (I), the perforated plate modelled to the equivalent solid plate also experienced both plastic and creep deformations. The locus of yield surface for the two portion is presented in Fig 6. The yield surface is found to move slightly towards axial or hoop direction for portion (I) and (II) respectively. One example of the hysteresis loop obtained by inelastic analysis for portion (I) is shown in Fig.7. The uniaxialized hysteresis loop for this portion is shown in Fig.8 in comparison with the hysteresis loop which is assumed in the elastic-analisis-based evaluation. Highly larger strain range than that by inelastic analysis is assumed in the case of elastic-analysis based estimation. Stress-time diagram of that portion is also shown in Fig.9, using both equivalent stresses by von Mises and Huddleston. Both stresses are not so high during the steady state operation, and the equivalent stress by Huddleston is somewhat lower than that by von Mises. The results of strengh evaluation for 100 cycles are summarized in Table 1. The analytical results for the third cycle is used for strength evaluation. Inelastic-analysis-based creep-fatigue damage by linear damage rule is far less than elastic-analysis based damage, exhibiting admissible damage with dominant fatigue damage and

negligible creep damage. The damage by SRP method is also less than the limit value of unity.

5. DISCUSSION

The applicability of the present constitutive model to both uniaxial and multiaxial state is demonstrated in the related paper(Igari & Koto et al. 1987). The features of the nonlinear plasticity model are found in the hysteresis loops in Fig.7. Translation of the yield surface by the creep strain during the steady state operation is seen in Fig.6, since plasticity-creep interaction on the translation of yield surface is considered in this model. The cyclic hardening of the material against three cycles of operation is found not to be significant due to small strain range. Prospective cyclic hardening for the number of cycle over 100 will be larger than that obtained here. Consequently, the present inelastic analysis predicts "softer" plastic response of the material than the representative response during whole life. This fact indicates that the fatigue damage based on the present inelastic analysis gives a conservative prediction, and that the creep damage obtained gives a unconservative prediction due to lower estimated stress than the representative response. In the present strength evaluation based on the linear damage rule with inelastic analysis, the damage for 100 cycles with dominant fatigue damage and negligible creep one is far less than the damage limit, and also far less than that by elastic analysis, where conservative assumptions are considered. Thus, even if the representative response is used for damage evaluation, the damage will be small that confirm the integrity of the structure. The estimation based on SRP method leads to a larger damage value than the linear damage rule. The treatment of multiaxiality and ratchetting is to be clarified in this method.

6 CONCLUDING REMARKS

Results of inelastic analysis and life assessment of intermediate heat exchanger in fast breeder reactor are presented in the paper. The possibility to describe the inelastic behavior of material more realistically than conventional method is shown. The reliability of the inelastic design of the high-temperature structures depends on the reliability of both inelastic constitutive model and life estimation method. Comparison with the experimental results of deformation and failure of structural model is a future work for this project.

REFERENCES

Corum,J.M. 1974. ORNL 5014

Huddleston,R.L. 1985. ASME PVT. 107 : 421-429

Igari,T., Koto,H., Wada,H. & Asada,Y. 1987. Trans. SMiRT-9. L3/6

Igari,T., Setoguchi,K. & Yamauchi,M. 1983. J. Soc. Mat. Sci. (in Japanese). 32:610-614

Igari,T., Setoguchi,K., Matsumura,N. & Nomura,S. 1987. Trans. SMiRT-9,. L4/4.

Manson,S.S. 1973. ASTM STP 520 : 744-782

Sakon,T., Wada,H. & Asada,Y. 1987. Trans. SMiRT-9, L6/7

van de Graaf,H., Thung,K.G. & Heslenfeld,M.W. 1985., Trans. SMiRT-8, E1/4

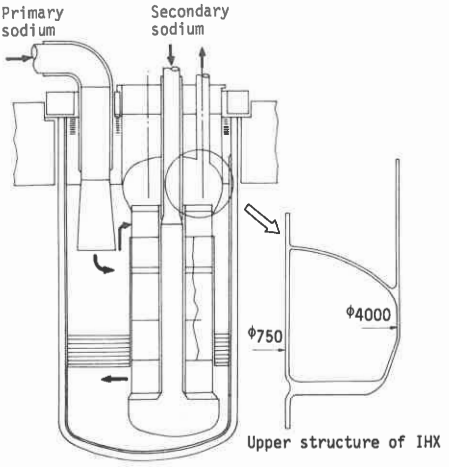

Fig. 1 Schematic view of intermediate heat exchanger

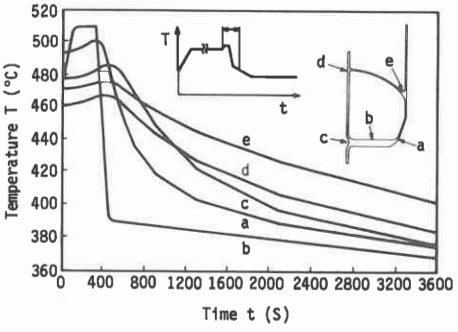

Fig. 4 Time history of temperature at hot shock and down shock

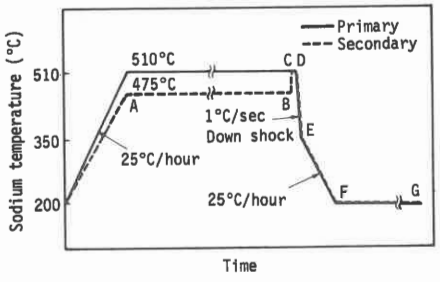

Fig. 2 Operation curve used for analysis (Manual trip)

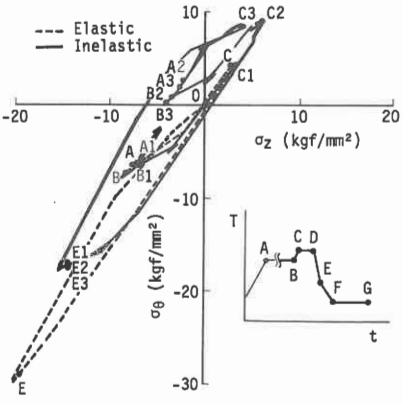

(a) Portion (I)

Fig. 5-1 Stress trajectries for representative portions

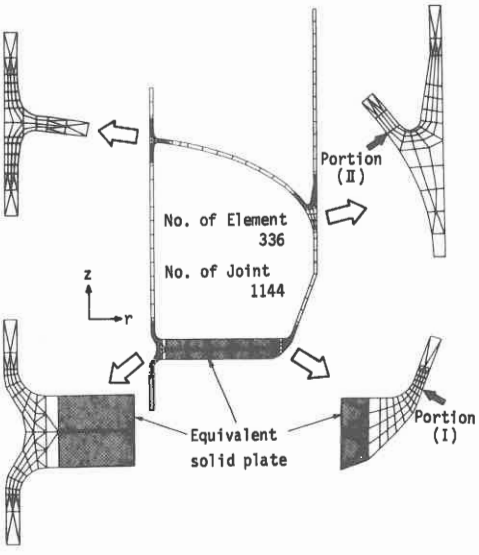

Fig. 3 Mesh division (Axisymmetric body)

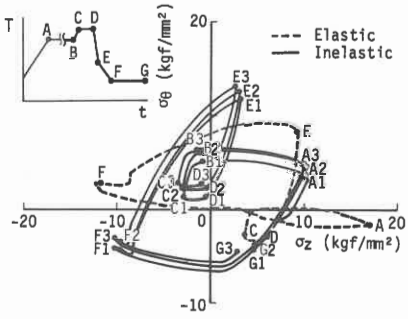

(b) Portion (II)

Fig. 5-2 Stress trajectries for representative portions

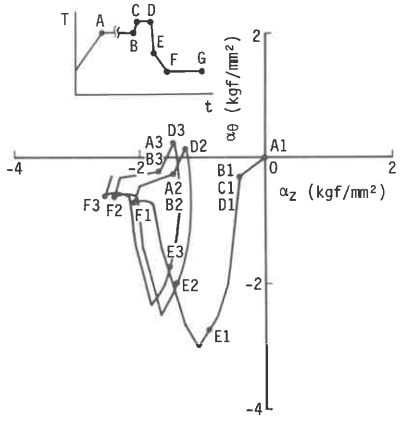

(a) Portion (I)

Fig. 6-1 Trajectries of center of yield surface for representative portions

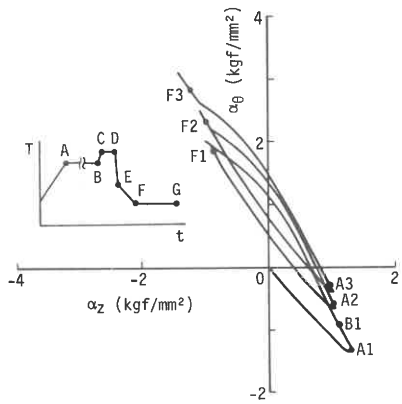

(b) Portion (II)

Fig. 6-2 Trajectries of center of yield surface for representative portions

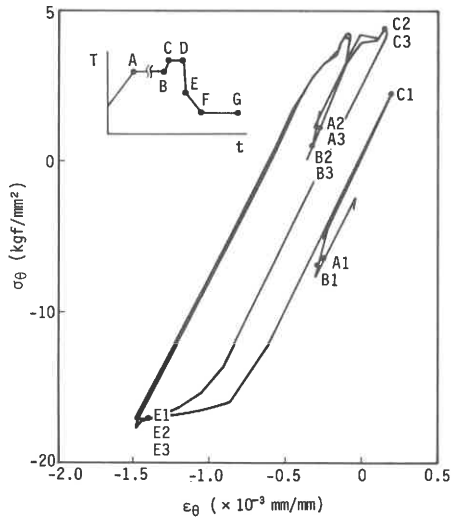

Fig. 7 Example of hysteresis loop for portion (I)

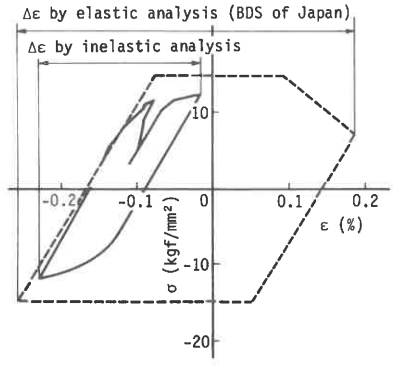

Fig. 8 Uniaxialized hysteresis loop for portion (I)

Table 1 Result of strength estimation

		Portion (I)	Portion (II)
Elastic	S_n(kgf/mm²)	39.1	52.9
	D_f	0.237	1.041
	D_c	1.763	2.072
	$D_f + D_c$	2.000	3.113
Inelastic	D_f	0.003	0.045
	D_c	0.000	0.000
	$D_f + D_c$	0.003	0.045
	ω*	0.021	0.032
	SRP**	0.051	0.319

* : Creep ductility consumption (Limit : 1.0)

** : Interaction damage rule (Limit : 1.0)

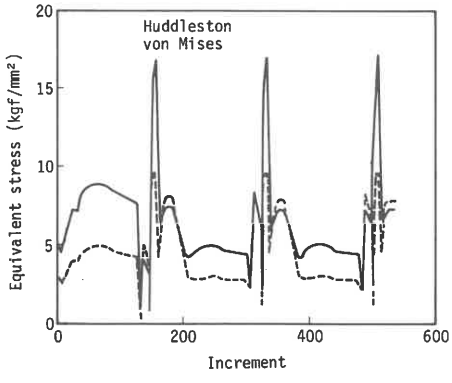

Fig. 9 Example of time history of equivalent stress for portion (I)